Chapter 4

Template synthesis and spectral characterization of quinoxaline–2–carboxalidine–L–histidine complexes of manganese(II), iron(III), cobalt(II), nickel(II), copper(II) and zinc(II)

Contents

4.1 INTRODUCTION

Complexes of Schiff bases derived from amino acids attract chemists and biologists due to their interesting and useful pharmacological and biological properties [1-3]. They can be taken as good models to study metal-ligand interactions in metalloproteins and metalloenzymes. L-Histidine (Figure 4.1) serves as a ligand through the imidazole imido nitrogen atom in many enzymes.

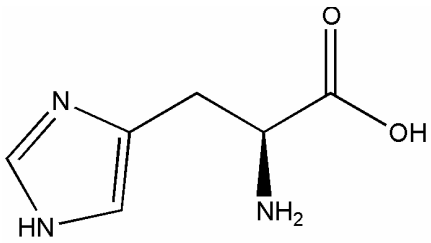

Figure 4.1: ***Structure of L-histidine***

The formation of Schiff base intermediates in reactions of biological importance is well documented [4, 5]. We report here a convenient synthesis of few

Schiff base complexes via template method under mild reaction conditions. The routine use of metal template procedures for obtaining a wide range of compounds stems from 1960, when Curtis discovered a template reaction for obtaining an isomeric pair of nickel macrocyclic complexes [6]. Template effect may arise from stereochemistry imposed by metal ion coordination of some of the reactants. It promotes a series of controlled steps and characteristically provides routes to products not formed in the absence of the metal ion [7, 8]. The metal ion may sequester the cyclic product from an equilibrium mixture promoting the formation of the metal complex or it may direct the steric course of a condensation facilitating the formation of the required cyclic product [9, 10]. The template synthesis of transition metal complexes of the Schiff base derived from glycine and quinoxaline–2–carboxaldehyde was already reported from our group [11]. In continuation of this work, we have studied the synthesis and characterization of manganese(II), iron(III), cobalt(II), nickel(II), copper(II) and zinc(II) complexes of a Schiff base derived from quinoxaline–2–carboxaldehyde and L–histidine.

4.2 EXPERIMENTAL

4.2.1 Materials and methods

The method of preparation of quinoxaline-2-carboxaldehyde and the techniques employed for the characterization of metal complexes are given in chapter II.

4.2.2 Preparation of Complexes

Since ligand cannot be isolated for the synthesis of complexes, template method is adopted. In this method aldehyde, amine and metal compound are refluxed in 1:1:1 molar ratio. The general scheme of the reaction (Scheme 4.1) and procedural details are given below.

4.2.2.1. Preparation of the Mn(II), Fe(III), Co(II) and Ni(II) complex

The preparation of the Mn(II) complex was carried out by taking quinoxaldehyde (1.580 g, 0.01 mol) in methanol (30 mL) and L-histidine (1.550 g, 0.01 mol) in water (20 mL). To this solution, sodium acetate in methanol (5 mL) was added to adjust the pH around 9. The mixture was then refluxed on a water bath for half an hour. The colour of the solution turns from pale yellow to dark brown. To this hot solution, manganese acetate tetrahydrate (1.979 g, 0.01 mol) in methanol (20 mL) was added. The solution was refluxed for two more hours and then was kept at room temperature (28±2 °C). The precipitate formed was filtered and washed with methanol containing water and then with acetone. Fe(III), Co(II) and Ni(II) complexes were prepared in a similar way by using ferric chloride anhydrous (1.622 g, 0.01 mol), cobalt acetate hexahydrate (2.490 g, 0.01 mol) or nickel acetate hexahydrate (2.488 g, 0.01 mol).

4.2.2.2. Preparation of the Cu(II)and Zn(II) complex

Quinoxaldehyde (1.580 g, 0.01mol) in methanol (50 mL) was added to L-histidine (1.550 g, 0.01 mol) in water (30 mL). The solution was then refluxed on a water bath for half an hour. The colour of the solution turns from pale yellow to dark brown. To this hot solution, copper chloride (1.700 g, 0.01 mol) or zinc acetate (2.190 g, 0.01 mol) in methanol (20 mL) was added. Instantaneous formation of a precipitate was observed, and the refluxing was continued for one more hour to ensure complete precipitation. The precipitate was filtered and washed with methanol containing water and then with acetone.

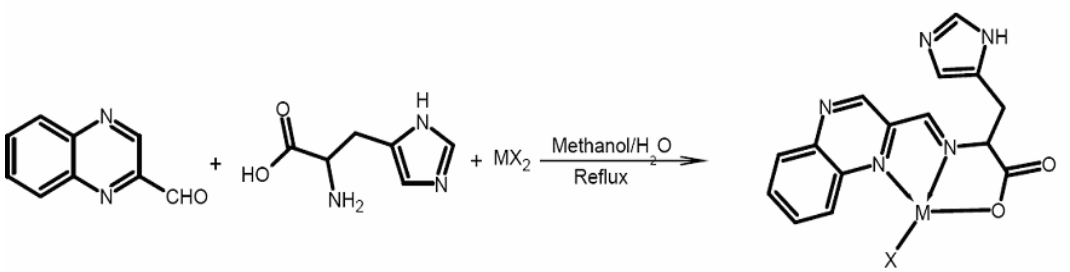

Scheme 4.1: ***The general scheme showing the formation of Schiff base complex of quinoxaline-2-carboxalidine-L-histidine by template method.***

4.3 RESULTS AND DISCUSSION

The complexes are found to be stable in air and non-hygroscopic. They are soluble in DMSO and DMF. The elemental analysis data of the complexes are given in Table 4.1. The data agree with the molecular formula of the complexes given in the Table. The molar conductivity measurements of all the complexes in DMF (10^{-3} M solution) have values in the range 5–25 $ohm^{-1}cm^2mol^{-1}$, which suggest the non-electrolytic nature of the complexes (Table 4.2). This further suggests that the anions are associated in the first coordination sphere of the complexes [12].

Table 4.1: ***Analytical data of complexes of qlh***

Compound	Colour	Yield (%)	Analytical data. Found (calculated) %				
			C	H	N	M	Cl
$[Mn(qlh)(OAc)].\ 2H_2O$	Black	55	46.07 (45.96)	4.25 (4.31)	15.41 (15.76)	12.86 (12.37)	–
$[Fe(qlh)Cl_2(H_2O)].\ H_2O$	Black	70	40.05 (39.42)	2.98 (3.53)	15.41 (15.32)	12.11 (12.22)	15.73 (15.51)
$[Co(qlh)(OAc)].2H_2O$	Black	62	45.51 (45.55)	3.97 (4.27)	15.86 (15.62)	12.79 (13.15)	–
$[Ni(qlh)(OAc)(H_2O)_2].H_2O$	Black	65	43.42 (43.81)	4.69 (4.54)	15.19 (15.03)	12.81 (12.59)	–
$[Cu(qlh)Cl].\ 2H_2O$	Black	80	41.54 (41.96)	3.32 (3.76)	16.36 (16.31)	15.09 (14.80)	8.45 (8.26)
$[Zn(qlh)(OAc)].2H_2O$	Red	80	44.87 (44.90)	4.09 (4.21)	15.48 (15.40)	14.47 (14.38)	–

Table 4.2*: Conductivity and magnetic moment data of the complexes*

Compound	μ_{eff} (B.M)	$\lambda_m^{\#}$
$[Mn(qlh)(OAc)].\ 2H_2O$	5.96	7
$[Fe(qlh)Cl_2(H_2O)].\ H_2O$	5.30	15
$[Co(qlh)(OAc)].2H_2O$	3.96	11
$[Ni(qlh)(OAc)(H_2O)_2].H_2O$	2.97	18
$[Cu(qlh)Cl].\ 2H_2O$	2.10	9
$[Zn(qlh)(OAc)].2H_2O$	–	5

$^{\#}$ Molar conductivity (in Mho $cm^2\ mol^{-1}$), 10^{-3} Molar solution in DMF

4.3.1 Magnetic susceptibility measurements

The room temperature (28±2 °C) magnetic moments of the complexes are given in Table 4.2. The μ_{eff} value of the Mn(II) complex was found to be 5.96 B.M. at room temperature as expected for a high spin d^5 system. The magnetic moment of $[Fe(qlh)Cl_2(H_2O)]$ is found to be 5.83 B.M. Hence the iron(III) like manganese(II) is high spin in its complex. The room temperature magnetic moment of the cobalt(II) complex is 4.66 B.M. which indicates a tetrahedral geometry around cobalt atom. The magnetic moment of the nickel(II) complex is found to be 3.32 B.M., which is as expected for an octahedral complex. The magnetic moment of the copper(II) complex is 1.92 B.M. which suggests the lack of Cu–Cu interactions and monomeric nature of the complex. The value also indicates that the molecules are in a magnetically dilute state and therefore the possibility of spin-spin coupling could be ruled out.

4.3.2 Infrared spectra

As we were not able to isolate the free ligand, the assignments of the infrared bands of the complexes are done based on the infrared spectra of the histidine and quinoxaline–2–carboxaldehyde. The IR spectra of the complexes are given in Figures 4.2–4.7. Most of the bands due to the quinoxaline–2–carboxaldehyde and histidine are present in the spectra of the complexes. However, the C=O stretching observed in quinoxaline–2–carboxaldehyde at 1680 cm^{-1} is absent in the spectra of complexes. This confirms the formation of Schiff base. The important IR spectral bands are listed in Table 4.3. The most characteristic IR spectral bands appear at 1610–1660 cm^{-1} as a multiplet which are attributable to asymmetric stretching of $\nu(COO^-)$ and ν(C=N) stretching of the azomethine moiety [13]. The symmetric $\nu(COO^-)$ stretching is observed around 1400–1420 cm^{-1} [14]. All the complexes show a broad absorption band around 3300 cm^{-1} due to the presence of water molecule. The (N–H) stretching of imidazole ring occurs in the

same region. However, due to overlap we could not differentiate them. The (C=N) stretching of quinoxaline ring occurs at 1550–1590 cm^{-1}. The low frequency vibrations observed around 400 cm^{-1} are due to metal–nitrogen and metal–oxygen stretching.

Table 4.3: ***IR spectral data of complexes of qlh***

Assignments	ν(H_2O), ν(NH)	ν(COO^-) $^{\$}$	ν(COO^-) $^{@}$	ν(C=N)$^{\#}$	ν(C=N) $^{\#\#}$	ν(M–O)	ν(M–N)
[Mn(qlh)(OAc)]. $2H_2O$	3330 b	1652	1416	1613	1571	446	409
[Fe(qlh)Cl_2(H_2O)]. H_2O	3300 b	1640	1412	1617	1541	440	414
[Co(qlh)(OAc)].$2H_2O$	3300 b	1645	1409	1613	1581	442	416
[Ni(qlh)(OAc)(H_2O)$_2$].H_2O	3397, 3361	1650	1407	1613	1579	440	420
[Cu(qlh)Cl]. $2H_2O$	3505, 3421	1642	1404	1621	1556	435	413
[Zn(qlh)(OAc)].$2H_2O$	3300 b	1653	1417	1621	1586	446	415

$^{\#}$ azomethine , $^{\#\#}$ quinoxaline , $^{@}$ symmetric stretching, $^{\$}$ asymmetric stretching

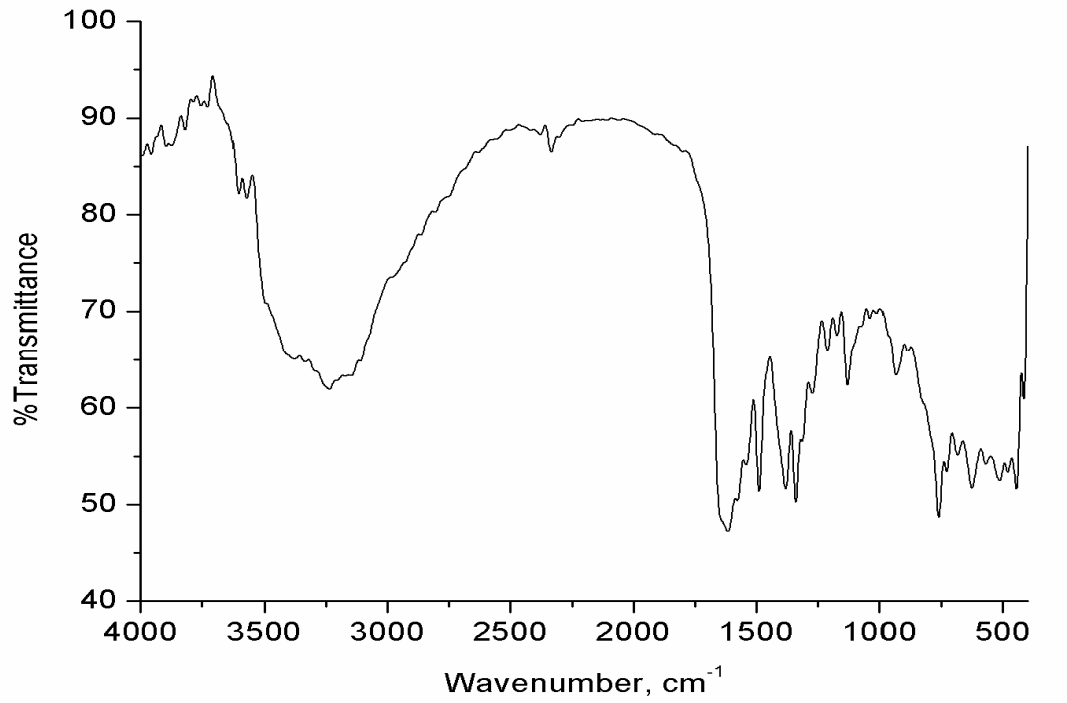

Figure 4.2: ***FTIR spectrum of [Mn(qlh)(OAc)]. $2H_2O$***

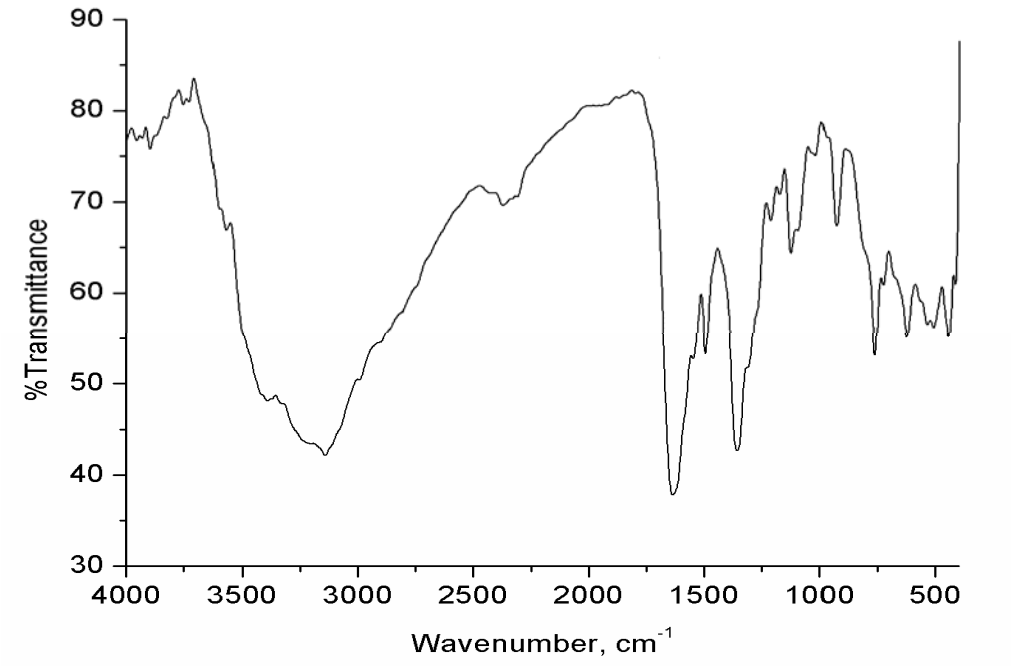

Figure 4.3: ***FTIR spectrum of [Fe(qlh)Cl$_2$(H$_2$O)]. H$_2$O***

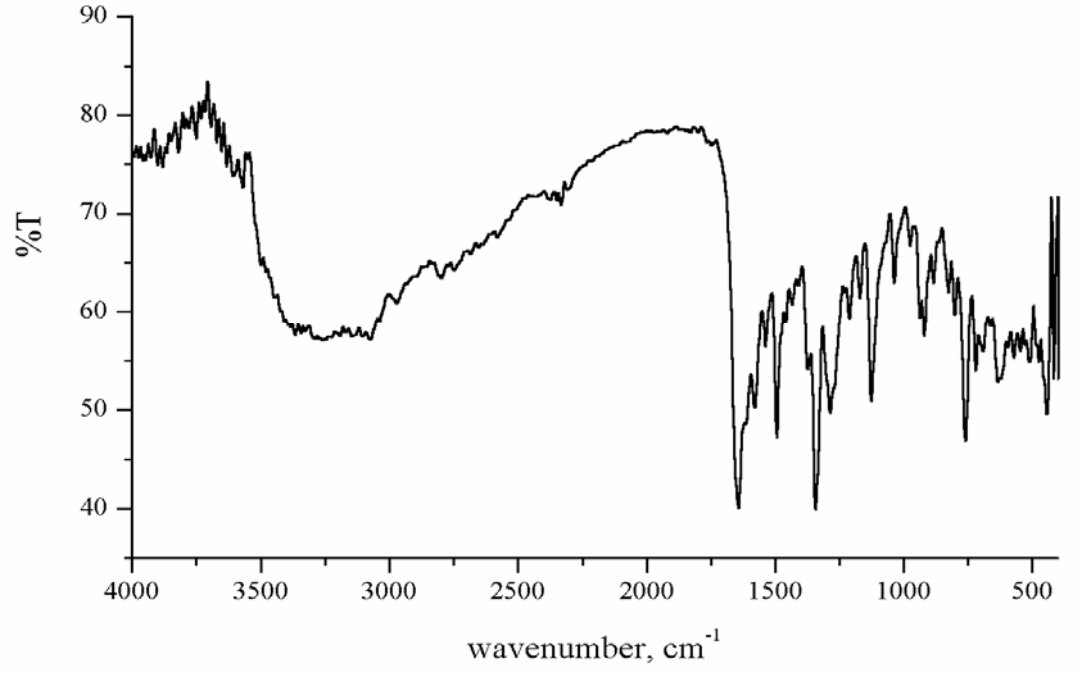

Figure 4.4: ***FTIR spectrum of [Co(qlh)(OAc)].2H$_2$O***

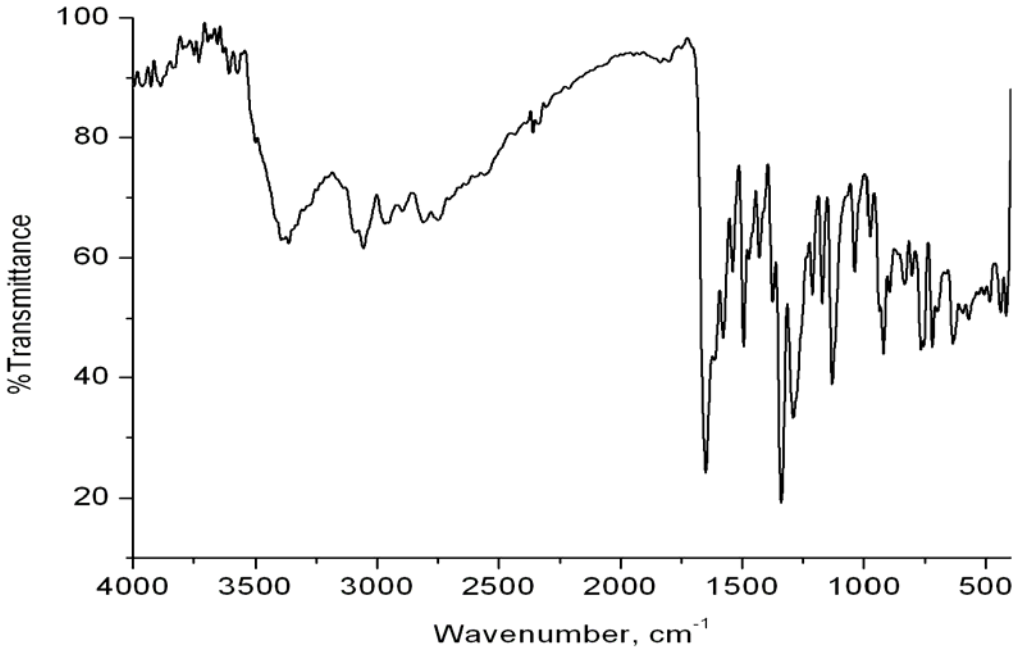

Figure 4.5: ***FTIR spectrum of [Ni(qlh)(OAc)(H$_2$O)$_2$].H$_2$O***

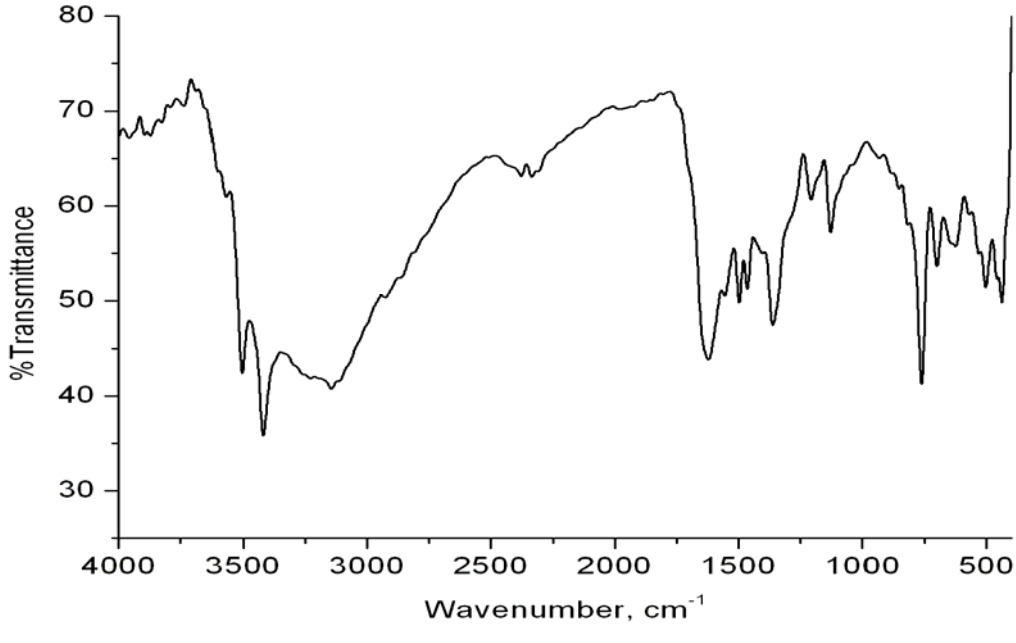

Figure 4.6: ***FTIR spectrum of [Cu(qlh)Cl]. 2H$_2$O***

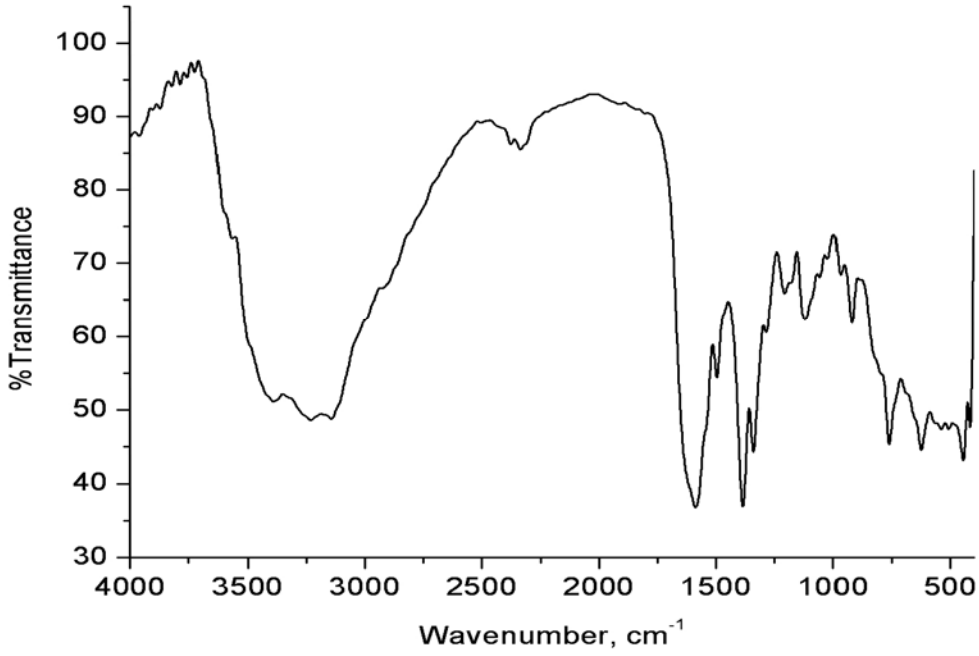

Figure 4.7: ***FTIR spectrum of [Zn(qlh)(OAc)].2H$_2$O***

4.3.3 Electronic spectra

The UV–Vis spectra of the Schiff base complexes in methanol (~5x10^{-4} molar) were recorded in the range 50000-10000 cm^{-1}, and are given in Figures 4.8–4.13. The spectral bands and their assignments are listed in Table 4.4. For all the complexes the bands observed between 28500 to 50000 cm^{-1} are identical and might be due to π–π* transitions and intraligand charge transfer transitions of quinoxaline ring, imidazole ring and azomethine C=N moiety. The forbidden n–π* transitions are not observed.

The electronic transitions from $^6A_1$ ground state of manganese(II) to higher energy states are spin-forbidden and these transitions are difficult to observe in the spectrum. The spectrum of [Mn(qlh)(OAc)] contains bands at 27550 and 20200 cm^{-1}, which corresponds to $^6A_1 \rightarrow {}^4E_1(D)$ and $^6A_1 \rightarrow {}^4T_1(G)$ transitions. Similar observations has been made in the case of tetrahedral manganese(II) complexes [15, 16].

The ground state of high spin octahedral Fe(III) complexes is $^6A_{1g}$. The four lowest energy bands are expected for such complexes the transition from $^6A_{1g}$ to $^4T_{1g}$, $^4T_{2g}$, ^4E_g, and $^4A_{1g}$, excited states. The Fe(III) complex exhibits only a charge transfer band at 27700 and a weak shoulder at 24400 cm^{-1}. The charge transfer band might have obscured the weak forbidden d-d transitions. However, the shoulder band might be due to the $^6A_{1g} \rightarrow {}^4T_{1g}$ transition expected for the iron(III) octahedral complexes [17].

The spectrum of the cobalt(II) complex contains a d-d band at 16670 cm^{-1}, which corresponds to $^4A_2 \rightarrow {}^4T_1(P)$ transitions [15]. There is a charge transfer band at 27400 cm^{-1}. In addition to the solution spectrum, the spectrum of the cobalt(II) complex is taken in nujol to get more information about the geometry around cobalt. The geometry can be distinguished by analyzing the near IR region of the electronic spectrum. The low-energy multiplets at 8000 and 7500 cm^{-1} in the mull spectrum indicates the tetrahedral geometry of the cobalt(II) complex and this band might be due to $^4A_2(F) \rightarrow {}^4T_1(F)$ transition [18, 19]. The electronic spectrum of the cobalt(II) complex in nujol mull is presented in Figure 4.14.

Spectrum of the nickel(II) complex exhibits three shoulders at 23600, 17760 and 9800 cm^{-1} which indicates an octahedral geometry around nickel atom [20] and these bands corresponds to $^3A_{2g} \rightarrow {}^3T_{2g}$, $^3A_{2g} \rightarrow {}^3T_{1g}$ and $^3A_{2g} \rightarrow {}^3T_{1g}(P)$ transitions respectively.

The spectrum of [Cu(qlh)Cl].$2H_2O$ gives a weak broad band in the visible region, 13000 to 19000 cm^{-1} assignable to $^2B_{1g} \rightarrow {}^2E_g$ transition. The bands at 25900 and 15500 cm^{-1} correspond to $^2B_{1g} \rightarrow {}^2A_{1g}$ and $^2B_{1g} \rightarrow {}^2E_g$ transitions. It indicates the square planar geometry of the complex around copper atom [15, 21]. The zinc(II) complex exhibits only an intra ligand charge transfer transition at 31250 cm^{-1}. No d-d transitions are expected for d^{10} zinc complexes.

Table 4.4: ***UV-Vis spectral data of the complexes in methanol***

Compound	Absorption maxima cm^{-1}	log ε (ε in L mol^{-1} cm^{-1})	Tentative assignments
[Mn(qlh)(OAc)]. $2H_2O$	42000	3.36	π–π*
	31650	2.89	π–π*
	27550	2.08	$^6A_1 \rightarrow {}^4E(D)$
	20200	1.90	$^6A_1 \rightarrow {}^4T_1(G)$
[Fe(qlh)Cl_2].$2H_2O$	41700	3.72	π–π*
	31050	3.23	π–π*
	27700	3.20	CT
	24400	1.95	$^6A_{1g} \rightarrow {}^4T_{1g}$
[Co(qlh)(OAc)].$2H_2O$	40000	3.37	π–π*
	27400	3.14	CT
	16670	1.95	$^4A_2 \rightarrow {}^4T_1(P)$
	8000*		$^4A_2 \rightarrow {}^4T_1(F)$
	7500*		
[Ni(qlh)(OAc)(H_2O)$_2$].H_2O	39840	3.53	π–π*
	27300	3.27	CT
	23600	1.60	$^3A_{2g} \rightarrow {}^3T_{2g}$
	17760	1.48	$^3A_{2g} \rightarrow {}^3T_{1g}$
	9800	0.97	$^3A_{2g} \rightarrow {}^3T_{1g}(P)$
[Cu(qlh)Cl]. $2H_2O$	41700	3.75	π–π*
	31300	3.33	CT
	25900	2.47	$^2B_{1g} \rightarrow {}^2A_{1g}$
	15500	1.90	$^2B_{1g} \rightarrow {}^2E_g$
[Zn(qlh)(OAc)].$2H_2O$	42200	3.63	π–π*
	31250	3.24	CT

* in nujol

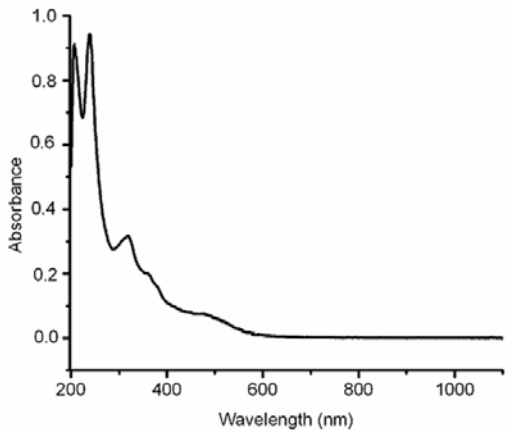

Figure 4.8: ***The UV-Vis spectrum of [Mn(qlh)(OAc)]. 2H_2O***

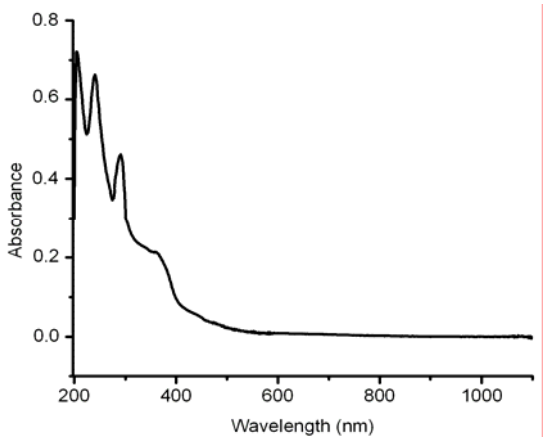

Figure 4.9: ***The UV-Vis spectrum of [Fe(qlh)Cl_2].2H_2O***

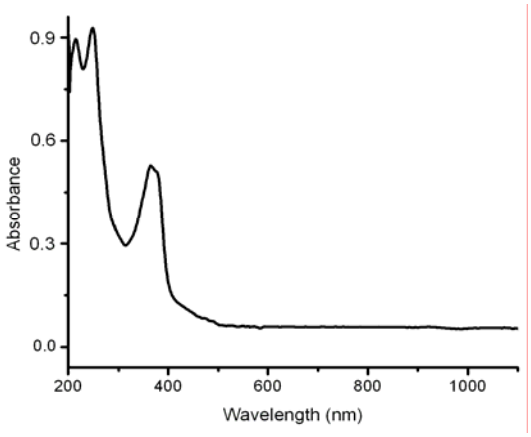

Figure 4.10: ***The UV-Vis spectrum of [Co(qlh)(OAc)].2H_2O***

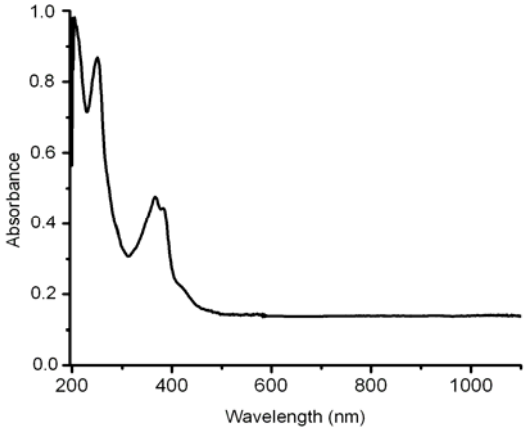

Figure 4.11: ***The UV-Vis spectrum of [Ni(qlh)(OAc)(H_2O)$_2$].H_2O***

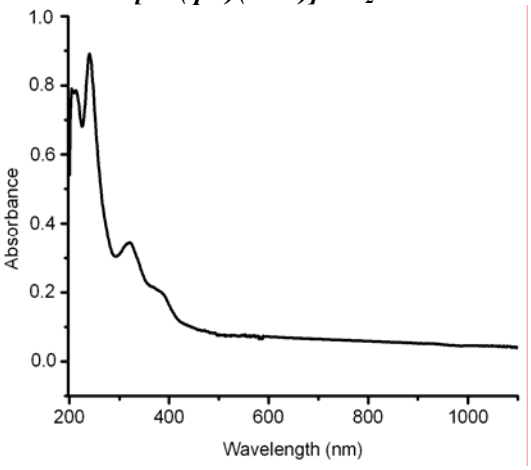

Figure 4.12: ***The UV-Vis spectrum of [Cu(qlh)Cl]. 2H_2O***

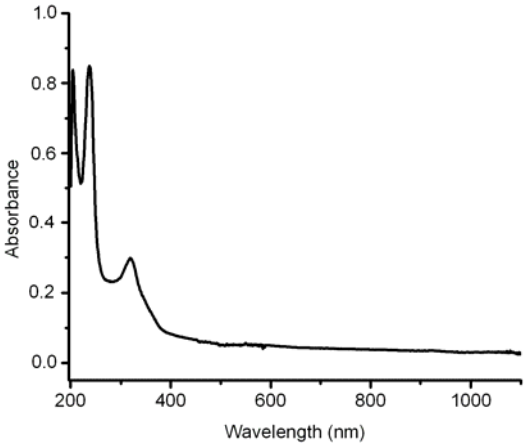

Figure 4.13: ***The UV-Vis spectrum of [Zn(qlh)(OAc)].2H_2O***

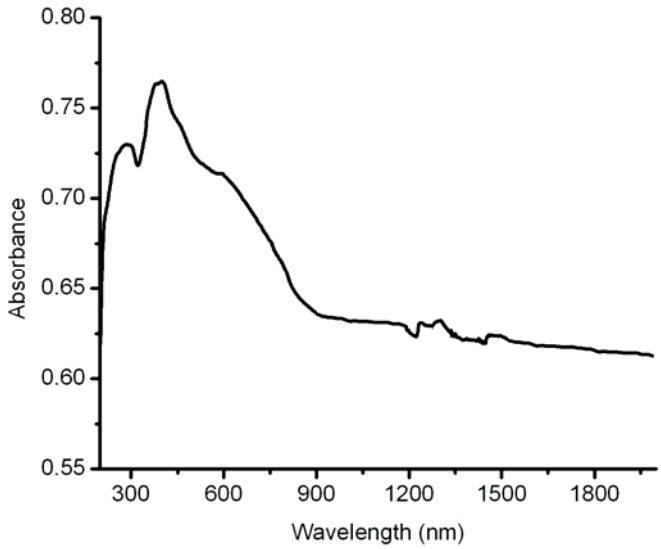

Figure 4.14: ***UV-Vis spectrum of [Co(qlh)(OAc)] in nujol mull***

4.3.4 Thermal analysis

There is weight loss below 120 ºC in all complexes suggesting the presence of lattice water molecules [22]. The thermogravimetric analysis data of the complexes upto 200 ºC give an indication about number and nature of water molecules in the complex (Table 4.5). A loss of one lattice water and two coordinated water molecules in the nickel(II) complex is observed in the temperature range 50-210 ºC. Above 350 ºC, the complexes begin to decompose and finally give the corresponding metal oxide. All the compounds are found to be thermally stable and exhibit multi stage decomposition pattern. The TG-DTG plots of the complexes are given in Figures 4.15–4.20. Thermal results show good agreement with the molecular formula arrived from the analytical data.

Table 4.5: The thermogravimetric analysis data below 200 ºC

Complex	Temperature range, ºC	% loss	Fragment lost	Nature of water lost
$[Mn(qlh)(OAc)].2H_2O$	60–120	8.3	2 H_2O	Lattice water
$[Fe(qlh)Cl_2(H_2O)].H_2O$	55–125	4.1	1 H_2O	Lattice water
	160–210	3.9	1 H_2O	Coordinated water
$[Co(qlh)(OAc)].H_2O$	60–120	4.3	1 H_2O	Lattice water
$[Ni(qlh)(OAc)(H_2O)_2].H_2O$	50–110	3.8	1 H_2O	Lattice water
	120–210	7.5	2 H_2O	Coordinated water
$[Cu(qlh)Cl].2H_2O$	70–140	8.5	2 H_2O	Lattice water
$[Zn(qlh)(OAc)].2H_2O$	50–130	7.9	2 H_2O	Lattice water

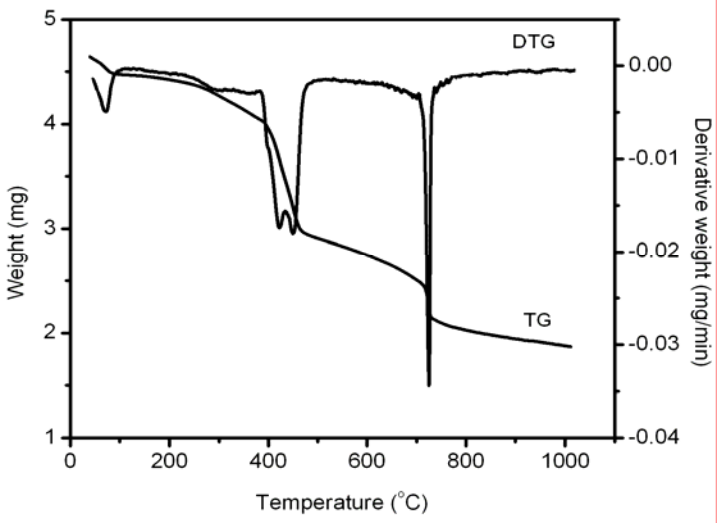

Figure 4.15: ***The TG/DTG plot of $[Mn(qlh)(OAc)].2H_2O$***

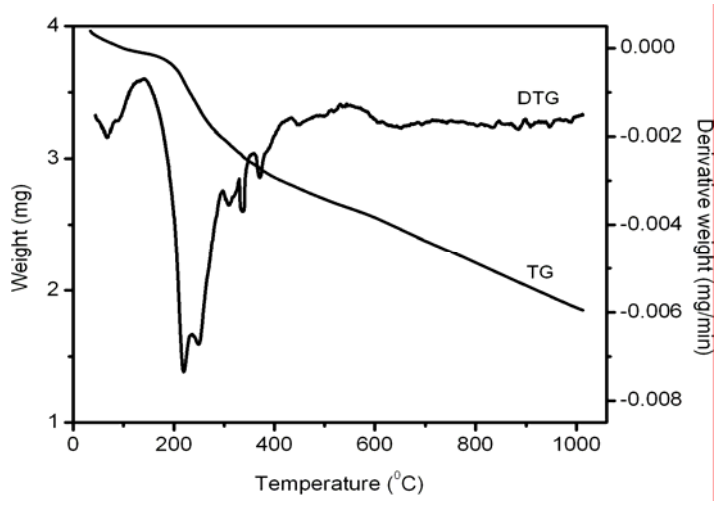

Figure 4.16: ***The TG/DTG plot of $[Fe(qlh)Cl_2(H_2O)].H_2O$***

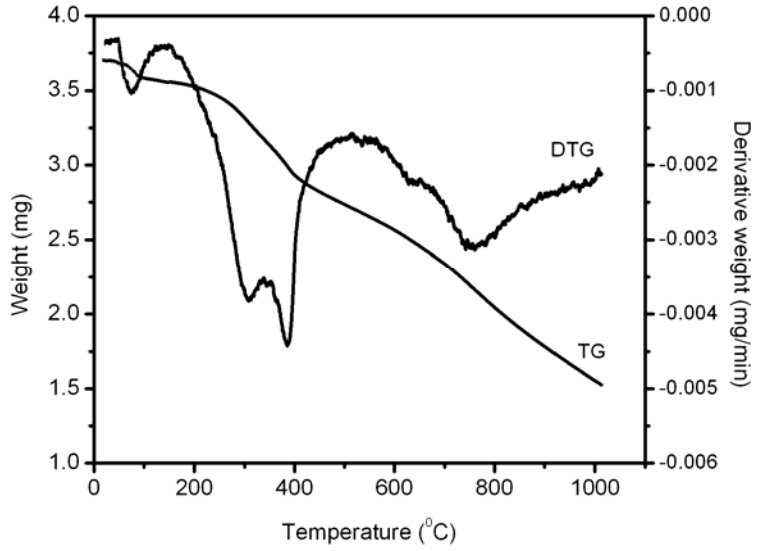

Figure 4.17: ***The TG/DTG plot of [Co(qlh)(OAc)].H_2O***

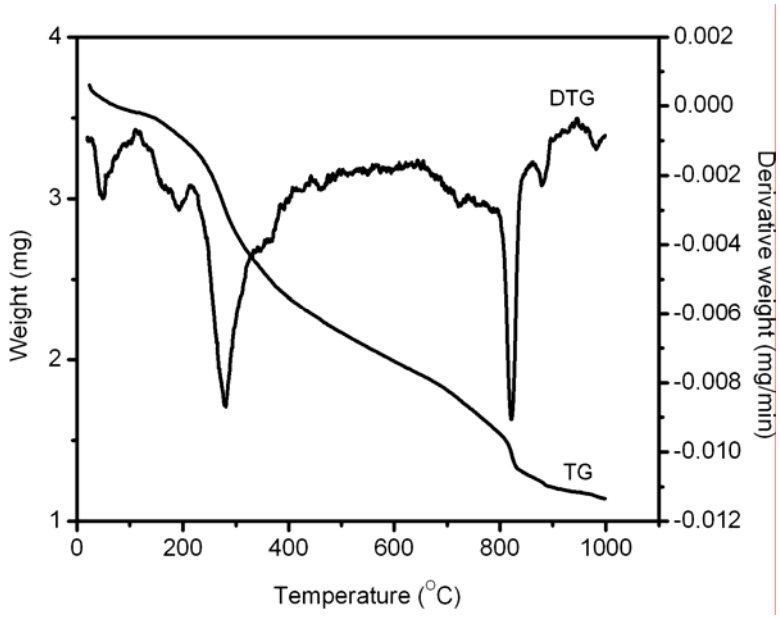

Figure 4.18: ***The TG/DTG plot of [Ni(qlh)(OAc)$(H_2O)_2$].H_2O***

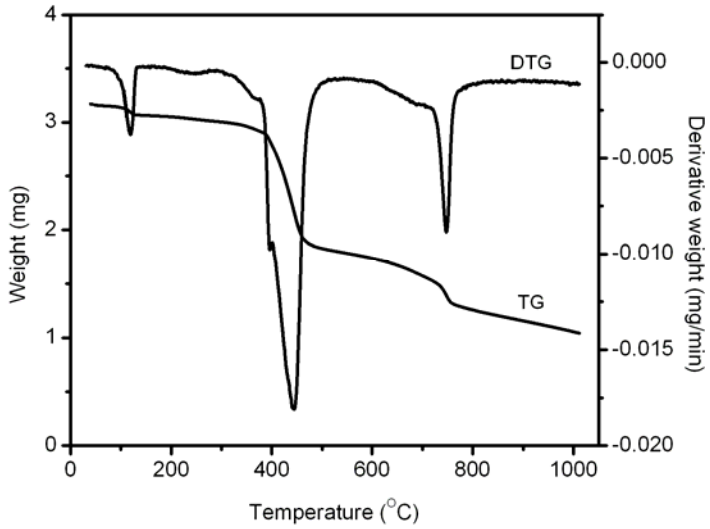

Figure 4.19: ***The TG/DTG plot of [Cu(qlh)Cl]. 2H₂O***

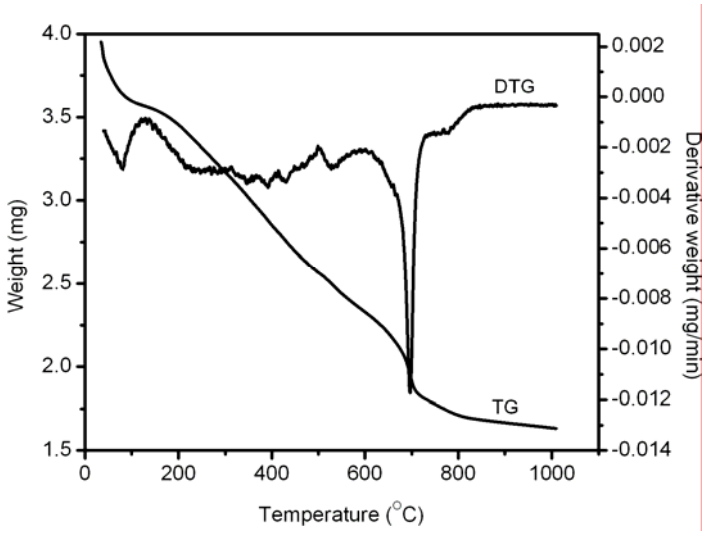

Figure 4.20: ***The TG/DTG plot of [Zn(qlh)(OAc)].2H₂O***

4.3.5 EPR spectra

The EPR spectrum of the Mn(II) complex in polycrystalline state gives a broad signal with a *g* value of 2.11. At room temperature (28±2 °C), Mn(II) complexes give very broad signals, which are due to dipolar interactions and enhanced spin lattice relaxation. The EPR spectrum of the manganese(II) complex in DMF at LNT exhibits six lines arising due to hyperfine interaction between the

unpaired electrons of the manganese(II) ion (I=5/2) with a g and A value of 1.99 and 0.00836 cm^{-1} respectively (Figure 4.21). This hyperfine spectrum of six lines corresponds to $m_I = \pm 5/2, \pm 3/2, \pm 1/2$, resulting from allowed transitions ($\Delta m_s = \pm 1$, $\Delta m_I = 0$).

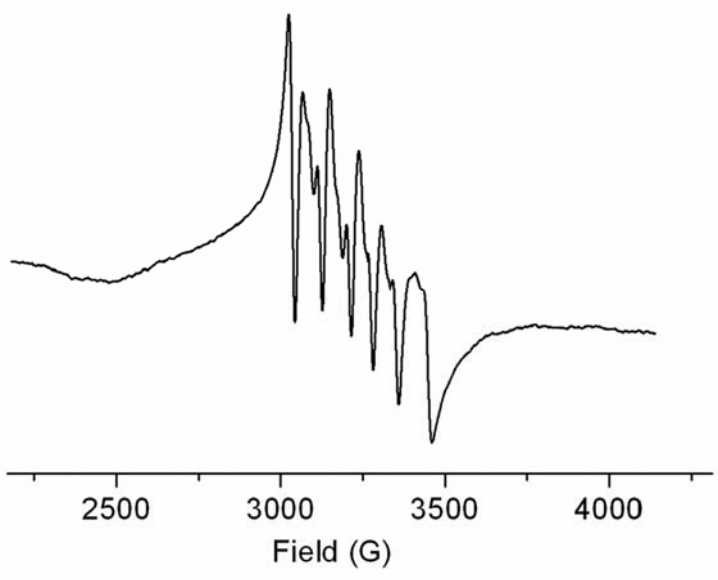

Figure 4.21: ***The EPR spectrum of [Mn(qlh)(OAc)(H$_2$O)$_2$].H$_2$O in DMF at LNT***

A pair of low intensity forbidden lines lying between each of the two main hyperfine lines is observed in the frozen solution spectra of the complexes. The forbidden lines in the spectrum arise due to the mixing of the nuclear hyperfine levels by the zero-field splitting factor of the Hamiltonian [23, 24].

In polycrystalline state EPR spectrum of the copper(II) complex gives an isotropic spectrum with a g value of 2.07. The EPR spectrum of the copper(II) complex in DMF at 77 K suggest that the copper(II) species is placed in two different environments [25]. The complicated nature of the spectrum is due to the presence of Cu(II) species in a square planar geometry and to those in octahedral geometry, which might be due to attachment of DMF (highly coordinating solvent) to the square planar species [26].

To overcome this problem, we repeated the spectral analysis in chloroform and got an axial spectrum with a $g_{\parallel}$ value of 2.21 and $g_{\perp}$ value of 2.07. The trend $g_{\parallel} > g_{\perp} > g_e$ (g_e is the g value of the free electron, 2.0023) observed for copper(II) complex shows that the unpaired electron is most likely localized in $d_x^2–d_y^2$ orbital of copper(II) ion and the features of the spectrum are characteristic of an axial symmetry [27, 28]. The EPR spectrum of the copper(II) complex in DMF and that in chloroform are presented in Figures 4.22 and 4.23 respectively.

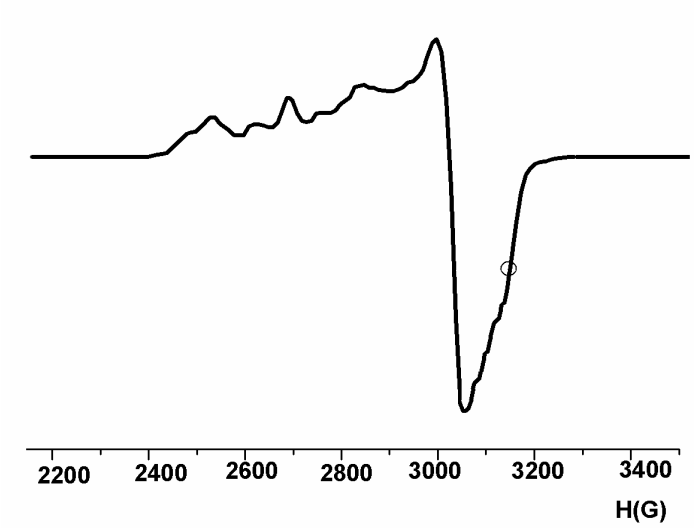

Figure 4.22: ***The EPR spectrum of [Cu(qlh)Cl].2H$_2$O in DMF at LNT***

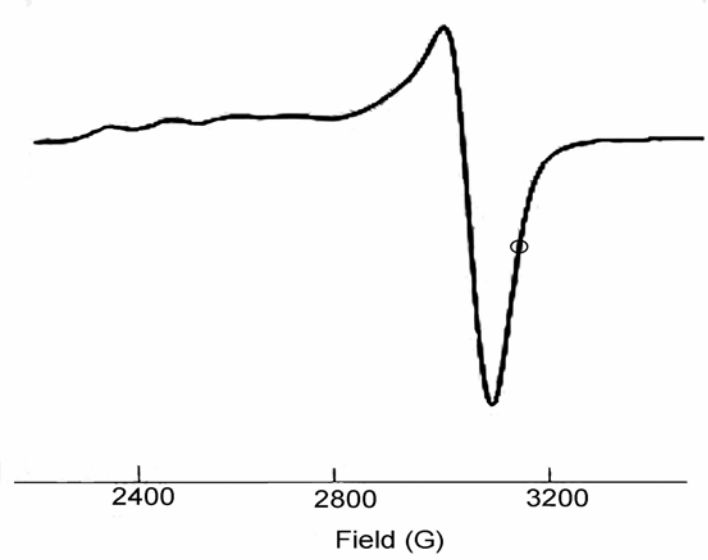

Figure 4.23: ***The EPR spectrum of [Cu(qlh)Cl].2H$_2$O in chloroform at LNT***

4.3.6 ^{1}H NMR spectrum of [Zn(qlh)(OAc)].2H_2O

The proton NMR spectrum of zinc(II) complex of qlh was taken in d_6-DMSO (Figure 4.24). The N-H proton resonates at 8.75 ppm [29], which is comparable to the reported value of histidine NH. Jacobsen [30] analyzed the NMR spectrum of an octapeptide which contains histidine as one of its building block. In the spectrum of peptide, the histidine NH resonates at 8.4 ppm. The protons of water molecules appear as a broad signal at 3.9–4.3 ppm. The aromatic protons appear as a multiplet at 7.60–8.50 ppm. The azomethine –CH proton appears as a singlet at 9.45 ppm, which is in the range expected for azomethines [31–34]. Imidazole ring protons resonate at 6.80–7.00 ppm. Acetate protons gave a chemical shift of 2.08 ppm. The spectral data of the zinc(II) complex is given in Table 4.6. The proton which is α to the amino and carboxyl moiety gives a chemical shift value of 2.70 ppm and the β protons resonates at 2.90 ppm.

Table 4.6: ***^{1}H NMR Spectroscopic data of [Zn(qlh)(OAc)].2H_2O***

Compound	Chemical shift, δ (ppm)	Assignment
[Zn(qlh)(OAc)].2H_2O	9.45	(s, 1H, azomethine)
	8.75	(s, 1H, NH)
	7.60–8.50	(m, 4H, Ar)
	6.80–7.00	(m, 2H, imidazole)
	3.9–4.3	(br, water of hydration)
	2.08	(s, 3H, acetate)
	2.70	(t, 1H, ali. histidine)
	2.90	(d, 2H, ali. histidine)

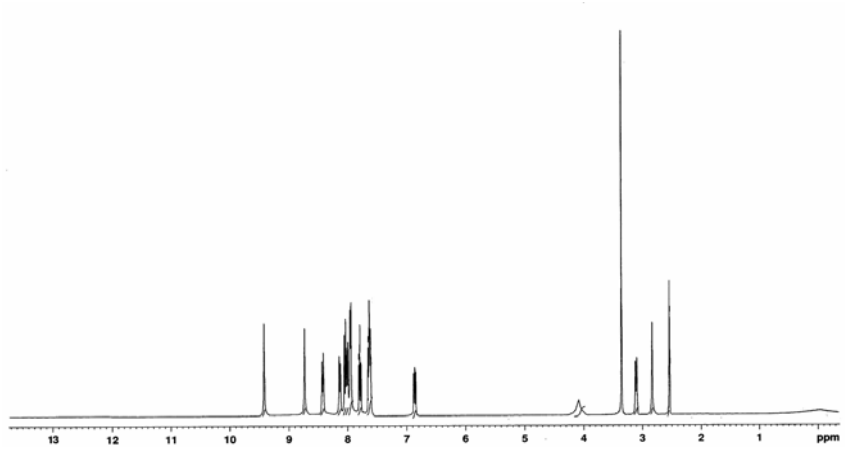

Figure 4.24: ***^{1}H NMR spectrum of [Zn(qlh)(OAc)].2H$_2$O***

4.4 CONCLUSIONS

In summary we have accomplished the facile synthesis of six complexes of the Schiff base quinoxaline–2–carboxalidine–L–histidine by template method and characterized them by elemental analysis, conductivity studies, magnetic susceptibility measurements, IR, UV–Vis, EPR and thermal analysis. The ligand qlh acts as a tridentate ligand. The physicochemical and spectral data reveal an octahedral geometry for the Fe(III) and Ni(II) complexes, a tetrahedral structure for manganese(II), cobalt(II) and zinc(II) complexes and a square planar geometry for the copper(II) complex. The proposed structures of the complexes are given in Figure 4.25.

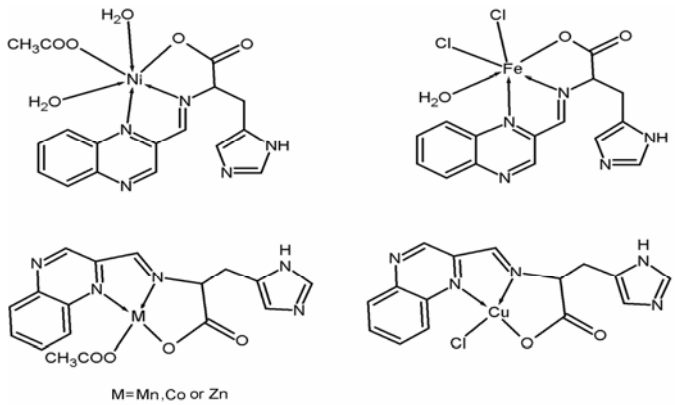

Figure 4.25: ***Suggested structures of the complexes of quinoxaline–2 carboxalidine–L–histidine (solvated water molecules are omitted)***

References

1. D. Sinha, A.K. Tiwari, S. Singh, G. Shukla, P. Mishra, H. Chandra, A.K. Mishra, *Eur. J. Med. Chem.* 43 (2008) 160.
2. R-M. Wang, C-J. Hao, Y-P. Wang, S-B. Li, *J. Mol. Catal. A: Chem.* 147 (1999) 173.
3. M.A. Neelakantan, F. Rusalraj, J. Dharmaraja, S. Johnsonraja, T. Jeyakumar, M.S. Pillai, *Spectrochim. Acta A* 71 (2008) 1599.
4. S.R. Collinson, D.E. Fenton, *Coord. Chem. Rev.* 148 (1996) 19.
5. H.S. He, D.T. Puerta, S.M. Cohen, K.R. Rodgers, *Inorg. Chem.* 44 (2005) 7431.
6. N.F. Curtis, *J. Chem. Soc.* (1960) 4409.
7. E.L. Blinn, D.H. Busch, *Inorg. Chem.* 7 (1968) 820.
8. M.C. Thompson, D.H. Busch, *J. Am. Chem. Soc.* 84 (1962) 1762.
9. D.H. Busch, C. Cairns, *Progress in Macrocyclic Chemistry*, Eds. R.M. Izatt, J. J. Christensen, John Wiley & Sons: New York, Vol. 3, (1987).
10. L.F. Lindoy, *The Chemistry of Macrocyclic Ligand Complexes*, Cambridge University Press: Cambridge (1989).
11. K.K.M Yusuff, R. Sreekala, *Synth. React. Inorg. Met. Org. Chem.* 21 (1991) 553.
12. W.J. Geary, *Coord. Chem. Rev*. 7 (1971) 81.
13. K. Nakamoto, *Infrared and Raman Spectra of Inorganic and Coordination Compound*, 5th Edn, Part B, John Wiley & Sons, London (1997).
14. D.L. Pavia, G.M. Lampman, G.S. Kriz, J.A. Vyan, *Introduction to spectroscopy*, Brooks Cole; 4th edition (2009).
15. A.B.P. Lever, *Inorganic Electronic Spectroscopy*, 2nd Edn, Elsevier, Amsterdam (1984).
16. F.A. Cotton, D.M.L. Goodgame, M. Goodgame, *J. Am. Chem. Soc.* 84 (1962) 167.

17. N.U. Shetty, V.K. Revankar, V.B. Mahale, *Proc. Indian Acd., Chem. Sci.* 109 (1997) 7.

18. D.M.L. Goodgame, M. Goodgame, *Inorg. Chem.* 4 (1965) 139.

19. S. Mayadevi, P.G. Prasad, K.K.M. Yusuff, *Synth.React. Inorg. Met. Org. Chem.* 33 (2003) 481.

20. F.A. Cotton, G. Wilkinson, C.A. Murillo, M. Bochmann, *Advanced Inorganic Chemistry*, sixth ed., Wiley, New York (1999).

21. A.A. El-Asmy, G.A.A. Al-Hazmi, *Spectrochim. Acta A* 71 (2009) 1885.

22. M.M. Omar, G.G. Mohamed, *Spectrochim. Acta A* 61 (2005) 929.

23. J.E. Huheey, E.A. Keiter, R.L. Keiter, *Inorganic Chemistry*, 4th edn., Addison-Wesley, New York (1993).

24. A. Sreekanth, M. Joseph, H-K. Fun, M.R.P. Kurup, *Polyhedron* 25 (2006) 1408.

25. I. Adato, A.H.I. Ben-Bassat, S. Sarel, *J. Phys. Chem.* 75 (1971) 3828.

26. R. Pogni, M.C. Baratto, A. Diaz, R. Basosi, *J. Inorg. Biochem.* 79 (2000) 333.

27. T.A. Khana, S.Naseem, S.N. Khan, A.U. Khan, M. Shakir, *Spectrochim. Acta A* 73 (2009) 622.

28. P.F. Rapheal, E. Manoj, M.R.P. Kurup, *Polyhedron* 26 (2007) 818.

29. I.A. Tolmacheva, I.V. Mashevskaya, A.N. Maslivets, *Rus. J. Org. Chem.* 38 (2002) 281.

30. N.E. Jacobsen, *NMR spectroscopy explained*, John Wiley & Sons, Inc., Hoboken, New Jersey, Pages 186-187, (2007).

31. D. Sanz, A. Perona, R.M. Claramunt, J. Elguero, *Tetrahedron* 61 (2005) 145.

32. K.K. Upadhyay, A. Kumar, S. Upadhyay, P.C. Mishra, *J. Mol. Str.* 873 (2008) 5.

33. G-Y. Yeap, S.-T. Ha, N. Ishizawa, K. Suda, P-L. Boey, W.A.K. Mahmood, *J. Mol. Str.* 658 (2003) 87.

34. T.Głowiak, L. Jerzykiewicz, J.M. Sobczak, J.J. Ziółkowski, *Inorg. Chim. Acta* 356 (2003) 387.